Title

Hepatic proteome analysis reveals altered mitochondrial metabolism and suppressed acyl-CoA synthetase-1 in colon-26 tumor-induced cachexia

Journal

Physiological Genomics, 52(5)

ISSN

1094-8341

Authors

Khamoui, Andy V
Tokmina-Roszyk, Dorota
Rossiter, Harry B
et al.

Publication Date

2020-05-01

DOI

10.1152/physiolgenomics.00124.2019

Peer reviewed

Hepatic proteome analysis reveals altered mitochondrial metabolism and suppressed acyl-CoA synthetase-1 in colon-26 tumor-induced cachexia

Andy V. Khamoui[1,2]*, Dorota Tokmina-Roszyk[2,3], Harry B. Rossiter[5,6], Gregg B. Fields[2,3,4], Nishant P. Visavadiya[1]

[1]Department of Exercise Science and Health Promotion, Florida Atlantic University, Boca Raton, FL, USA; [2]Institute for Human Health & Disease Intervention, Florida Atlantic University, Boca Raton, FL, USA; [3]Department of Chemistry & Biochemistry, Florida Atlantic University, Jupiter, FL, USA; [4]Department of Chemistry, The Scripps Research Institute, Jupiter, FL, USA; [5]Division of Respiratory and Critical Care Physiology and Medicine, Department of Medicine, The Lundquist Institute for Biomedical Innovation at Harbor-UCLA Medical Center, Torrance, CA, USA; [6]Faculty of Biological Sciences, University of Leeds, Leeds, UK

Running Title: Hepatic proteome in cancer cachexia

*Correspondence

Andy V. Khamoui PhD

Department of Exercise Science and Health Promotion

Florida Atlantic University

777 Glades Rd, FH-11A, Rm 128-B

Boca Raton, FL 33431

Tel: (561) 297-4450 | Email: akhamoui@fau.edu

Abstract

Cachexia is a life-threatening complication of cancer traditionally characterized by weight loss and muscle dysfunction. Cachexia, however, is a systemic disease that also involves remodeling of non-muscle organs. The liver exerts major control over systemic metabolism yet its role in cancer cachexia is not well-understood. To advance the understanding of how the liver contributes to cancer cachexia, we used quantitative proteomics and bioinformatics to identify hepatic pathways and cellular processes dysregulated in mice with moderate and severe colon-26 tumor-induced cachexia. ~300 differentially expressed proteins identified during the induction of moderate cachexia were also differentially regulated in the transition to severe cachexia. KEGG pathways enrichment revealed representation by oxidative phosphorylation, indicating altered hepatic mitochondrial function as a common feature across cachexia severity. Glycogen catabolism was also observed in cachexic livers along with decreased pyruvate dehydrogenase protein X component (Pdhx), increased lactate dehydrogenase A chain (Ldha), and increased lactate transporter Mct1. Together this suggests altered lactate metabolism and transport in cachexic livers, which may contribute to energetically inefficient inter-organ lactate cycling. Acyl-CoA synthetase-1 (ACSL1), known for activating long-chain fatty acids, was decreased in moderate and severe cachexia based on LC-MS/MS analysis and immunoblotting. ACSL1 showed strong linear relationships with percent body weight change and muscle fiber size (R^2=0.73-0.76, P<0.01). Mitochondrial coupling efficiency, which is compromised in cachexic livers to potentially increase energy expenditure and weight loss, also showed a linear relationship with ACSL1. Findings suggest altered mitochondrial and substrate metabolism of the liver in cancer cachexia, and possible hepatic targets for intervention.

Keywords: mitochondrial function, TMT, quantitative proteomics, bioinformatics, STRING

Introduction

Cancer cachexia is a life-threatening condition in which tumor-induced metabolic abnormalities lead to severe weight loss, skeletal muscle atrophy, and intolerance to anti-cancer treatment (10, 11). Approximately half of all cancer patients experience cachexia, with incidence rising to ~80% in advanced cancer patients (33). Although cachexia is believed to be directly responsible for ~20% of cancer-related deaths, this debilitating complication remains an under-appreciated issue in oncology (33). Nutritional support does not ameliorate cachexia due to the metabolic abnormalities present, and approved treatments options are currently unavailable, contributing to significant frustration among patients and their family members (10, 26).

While skeletal muscle remains the most widely studied organ in cancer cachexia, increasing attention has been devoted to the mechanistic roles of other organs such as adipose, bone, brain, heart, and liver, reflecting a greater appreciation for the systemic nature of the disease (25). The multi-organ involvement highlights the significant complexities of tumor-induced cachexia, and unraveling the root cause remains a challenge. Omics technologies offer a global, unbiased approach to identify regulators of the cachexic phenotype (15, 31). In various omics platforms, mechanisms distinguishing cachexic from healthy muscle have been identified in patient-derived tissues, pre-clinical models, and myotubes treated with tumor-conditioned media (5, 14, 27-29). These investigations report that cachexic skeletal muscle displays enriched ubiquitin-dependent protein degradation, loss of sarcomere structure, mitochondrial dysfunction, disrupted energy metabolism, and energetic stress, offering an explanation for skeletal muscle atrophy and the symptom of fatigue.

In contrast to skeletal muscle, the liver has been relatively unexplored in cancer cachexia despite exerting major control over systemic metabolism. Several lines of limited evidence point to an influential role of the liver in cachexia-associated muscle atrophy and weight loss. First, the liver participates in the systemic acute phase response to disease and infection by synthesizing acute phase proteins. In order to support the increased demand for acute phase protein synthesis, amino acids are mobilized and released from skeletal muscle, contributing to tumor-induced muscle atrophy (6). It is also suggested that uncoupling of mitochondrial oxidative phosphorylation (OXPHOS) in the liver in cancer cachexia contributes to inefficiency, heat production, increased metabolic rate, and weight loss (9, 25). Indeed, a recent report found cachexic liver mitochondria to have reduced respiratory control ratio and increased LEAK respiration, suggesting impaired

OXPHOS coupling efficiency (18). Greater hepatic heat production arising from mitochondrial uncoupling may increase whole body resting energy expenditure and contribute to unintended weight loss. Lastly, cachexic livers may demonstrate increased gluconeogenesis supported by amino acids mobilized from the catabolism of skeletal muscle (17). When hepatic gluconeogenesis was normalized using a PPARα agonist, tumor-bearing mice were protected against weight loss and muscle atrophy (17), implying that hallmark features of cancer cachexia can be mitigated by targeting hepatic metabolism.

To identify hepatic pathways and cellular processes associated with cancer cachexia, as well as candidate hepatic targets for therapeutic intervention, unbiased omics analysis of cachexic liver tissues are warranted. Here we used tandem mass tag (TMT)-based quantitative proteomics to identify differentially expressed hepatic proteins and dysregulated metabolic pathways during the induction and progression of colon-26 tumor-induced cachexia, a well-established pre-clinical mouse model (7). Bioinformatics identified functional enrichments associated with the different degrees of cachexia severity, while findings were validated with immunoblotting and biochemical assays.

Methods

Animals and design

Ten-week-old Balb/c males (Envigo) were randomly assigned to receive either an injection of sterile PBS or colon-26 (C26) tumor cells. A tumor growth period of three weeks is typically allowed to elapse before tissue collection in order for hallmark features of cachexia to occur (i.e. weight loss, muscle atrophy). To evaluate mechanisms of cachexia severity, tissue was collected from C26 mice between days 14-21 after tumor cell injection, and classified according to weight loss in accordance with previous literature (6, 34). The 4 groups included: 1) Tumor-free, weight-stable mice that were PBS injected (PBS-WS, n=4), 2) C26 mice with confirmed tumors that did not exhibit weight loss and were therefore weight-stable (C26-WS, n=6), 3) C26 mice with moderate cachexia (10% weight loss; C26-MOD, n=7), and 4) C26 mice with severe cachexia (≥20% weight loss; C26-SEV, n=6). These classifications were adapted from previous pre-clinical investigations (6, 34). Weight loss for each mouse was determined by the percentage change between carcass weight (i.e. tumor-free body weight) and body weight recorded on the day of cell injection. Mice were individually housed, provided *ad libitum* water and food (5L0D, protein 29% fat 13%, carbohydrate 58%, PicoLab Laboratory

Rodent Diet), and maintained on a 12:12 hr light:dark cycle. C26 mice may or may not exhibit reduced food intake depending on the source of the C26 cells and the phenotype it generates when transplanted *in vivo* (23). The C26 cells in this study were obtained from a cell bank that others have used to demonstrate no significant effect of C26 cancer cachexia on food intake (4). Approval was obtained by the Institutional Animal Care and Use Committee (#A16-39) before any procedures were performed. Body and organ weights, muscle fiber size, and mitochondrial respiration data from this cohort of C26 mice were reported previously (18) and were used here to establish relationships with proteomic analyses generated by liquid chromatography-tandem mass spectrometry (LC-MS/MS) and immunoblotting.

C26 tumor cell culture and injection

C26 cells were cultured in a humidified incubator with 5% CO_2 using media that contained RPMI 1640 with 1% penicillin/streptomycin (vol/vol) and 10% FBS (vol/vol) (CLS Cell Lines Service, Eppelheim, Germany). Culture media was replaced every two to three days. At sub-confluency, cells were harvested by incubation with trypsin (0.05%, Gibco) and pelleted by centrifugation. The supernatant was discarded and the pellet resuspended in sterile PBS. Viable cells were identified and counted in a hemocytometer by trypan blue staining and light microscopy. Mice assigned to C26 groups were injected subcutaneously in the upper back with a cell suspension containing 1×10^6 cells. Mice assigned to the control group were administered an equivalent volume of sterile PBS (8, 21).

Tissue collection

Mice were euthanized by overdose with ketamine/xylazine cocktail injected i.p. (300/30 mg/kg). Euthanasia was performed during a four-hour time window from 10:00 am to 2:00 pm to ensure consistency in the timing of tissue collection. In order to attain 10% and 20% weight loss in moderate and severe cachexia, respectively, body weight was routinely monitored following tumor cell injection. Based upon our previous experience, we expected a final tumor mass at necropsy of ~2g with severe cachexia (20% target weight loss), and a tumor mass of ~1g with moderate cachexia (10% target weight loss). These parameters were factored into routine weight monitoring because measurements of body weight made before euthanasia would be confounded by tumor weight. For the typical Balb/c adult male weighing 25g, a tumor mass of 1g would

represent ~3-4% of body weight. During routine monitoring, a mouse showing ~7% weight loss would be euthanized in anticipation of tumor mass accounting for ~3-4% of body weight. This enabled the target weight loss of 10% for the moderate cachexia group (C26-MOD), with tissue being collected on day 14 (n=4), 15 (n=1), 17 (n=1), and 21 (n=1). For mice with confirmed, palpable tumors but no weight loss (C26-WS), tissue was collected on day 14 (n=1), 20 (n=2), and 21 (n=3). For all mice with severe cachexia (C26-SEV, n=6), tissue was collected on day 21 post-injection. Mice were not food deprived overnight or immediately prior to tissue collection. Collected tissue samples were weighed, sectioned, snap frozen and stored at -80°C.

High-resolution respirometry

Mitochondrial respiration was measured *in situ* in fresh liver tissue as we previously described and reported (18). Briefly, duplicate sections of liver tissue weighing ~6 mg each were gently separated in BIOPS solution under a dissecting microscope. Mechanically separated samples were placed into the respirometer chambers (Oxygraph-2k, Oroboros Instruments) and analyzed by injection of substrates, uncouplers, and inhibitors to determine mass-specific oxygen flux ($pmol \cdot s^{-1} \cdot mg^{-1}$). Several indicators of mitochondrial coupling were derived from high-resolution respirometry experiments including the respiratory control ratio (RCR), an index of OXPHOS coupling efficiency, which was calculated by dividing complex I supported OXPHOS by complex I supported LEAK respiration. In addition, LEAK respiration was normalized to both maximal OXPHOS and electron transfer system (ETS) capacities, which were obtained from injection of complex I and II linked substrates and 5 mM ADP (OXPHOS) or 0.5 µM CCCP (ETS).

Sample preparation and TMT labeling

Harvested liver tissue was transferred to lysis buffer (8 M Urea, 1 mM phenylmethylsulfonyl fluoride, 1x protease inhibitor cocktail) and sonicated (SONICS VCX750; amplitude 35%; pulse on 1 sec; pulse off 3 sec; total processing time 3 min) to release cell contents. Protein quantitation was performed using the Pierce quantitative colorimetric assay kit at λ = 480 nm according to the manufacturer's instructions (cat# 23275, ThermoFisher Scientific, USA). 250 ug of total protein per sample were then reduced with 200 mM tris(2-carboxyethyl)phosphine at 56°C for 1 h followed by alkylation with 20 mM iodoacetamide at room temperature in the dark for 1 h. An equal amount of protein was used for each tryptic digestion (1:50 ratio of

trypsin:substrate) at 37 °C overnight after which time the reaction was quenched with 0.1% formic acid. Samples were then lyophilized and subsequently dissolved in 100 mM triethylammonium bicarbonate. Tryptic peptides, 50 ug per sample, were labeled with TMT reagents for 1 h at room temperature after which the reaction was quenched with 5% hydroxylamine. Samples from each group were combined with equal amounts of TMT labeled internal standard, which was comprised of a mixture of protein extracts from all 23 samples. The sample labeling scheme is shown in Supplementary Table S1. Each pooled sample was then fractionated using RP-HPLC (Waters 2695 HPLC System equipped with Thermo Betasil C18 column, 80Å, 10 mm x 250 mm, 5 µm) with the separation gradient set to 8-32% B in 60 min (flow rate = 1mL/min, 20°C; A: 0.1% formic acid in water; B: 0.1% formic acid in acetonitrile) to yield 6 fractions.

LC-MS/MS and data analysis

Fractionated peptides were further separated using Nanoflow UPLC: Ultimate 3000 nano UHPLC system (ThermoFisher Scientific, USA) equipped with a trapping column (PepMap C18, 100 Å, 110 µm x 2 cm, 5µm) and an analytical column (PepMap C18, 100 Å, 75 µm x 50 cm, 2 µm). LC linear gradient was set to 2-8% B in 3 min, 8 to 20% B in 50 min, 20-40% B in 26 min, and 40-90% B in 4 min (A: 0.1% formic acid in water; B: 0.1% formic acid in 80% acetonitrile) with flow rate = 250 nL/min at 20°C. Peptides were then analyzed with Q Exactive HF mass spectrometer (ThermoFisher Scientific, USA). Precursor ion range was set to 300.0-1650.0 with $6x10^4$ resolution at 200 m/z and MS/MS product range starting from 100 m/z. Data was acquired in data dependent acquisition mode with up to 20 most intense peptide ions from preview scan selected for MS/MS. From each group 6 raw MS files were searched against mouse protein database using Maxquant (1.5.6.5). Search parameters included carbamidomethylation of cysteine (fixed) and oxidation of methionine (variable) in protein modification; enzyme specificity was set to trypsin with maximum of 2 missed cleavages and mass tolerance of 10 ppm for precursor ion and 0.6 Da for MS/MS. Proteins were selected for further analysis based on ≥1 unique peptides identified. The false discovery rate (FDR) was set to <1%.

Tissue homogenate

For all other *in vitro* experiments, liver tissue homogenate was prepared as we recently described (18). Briefly, 250 mg liver tissue was excised and washed with ice-cold mitochondrial isolation buffer

(215 mM mannitol, 75 mM sucrose, 0.1% BSA, 20 mM HEPES, 1 mM EGTA, and pH adjusted to 7.2 with KOH). Subsequently, tissue was homogenized in 1 mL of mitochondrial isolation buffer using a manual Potter-Elvehjem tissue grinder. The tissue homogenate was frozen immediately at -80 °C for later biochemical assays and western blotting. Protein concentration was determined by BCA kit (Pierce, Rockford, Il, USA).

Biochemical assays

Hepatic galactose (cat# ab83382, Abcam), free fatty acid (cat# ab65341, Abcam), triglyceride (cat# ab65336, Abcam) and glycogen (cat# K646, Biovision) content, as well as α-glucosidase (cat# ab174093, Abcam) and acyl-CoA synthetase (cat# K184, Biovision) enzyme activity was assayed using commercially available kits according to the manufacturers' protocols. The α-glucosidase enzyme activity was measured spectrophotometrically at λ = 410 nm. For the remaining assays, fluorescence signals generated from samples were measured at $\lambda_{excitation}$ = 530 nm and $\lambda_{emission}$ = 590 nm filters by a Biotek Synergy HTX spectrofluorometer (Winooski, VT). All parameters were normalized against total protein concentrations.

Western blotting

For western blot analysis, 30 µg of protein homogenate was mixed with 4X Laemmli sample buffer (cat# 161-0747, Bio-Rad) containing 355 mM 2-mercaptoethanol and separated on SDS-polyacrylamide gel electrophoresis, using 4–20% Criterion™ TGX™ Precast gels (cat# 5671095, Bio-Rad). The gel proteins were transferred onto an Immun-Blot PVDF membrane and then blocked with 5% nonfat dry milk in TBST buffer (Tris-buffered saline, 0.1% Tween-20) for 1 hour at room temperature. The PVDF membrane was incubated with the following primary antibodies overnight on a shaker at 4 °C in 5% milk: mitochondrial OXPHOS complexes (I to V) mouse mAb cocktail (1:2000, cat#ab110413, Abcam), 4-hydroxynonenal rabbit polyAb (4-HNE, 1:1000 dilution, cat# ab46545, Abcam), long-chain acyl-CoA synthetase 1 (ACSL1, 1:2000 dilution, cat# 4047, Cell Signaling) and GAPDH rabbit mAb (1:5000 dilution, cat# 5174, Cell Signaling). GAPDH was taken as an internal protein loading control. After 3 times TBST wash, the membranes were incubated with appropriate horseradish peroxidase (HRP)-conjugated horse anti-mouse IgG (cat#7076, Cell Signaling) or goat anti-rabbit IgG (cat# 7074, Cell Signaling) secondary antibodies for an hour at room temperature. Further, membranes were washed 3 times in TBST and then incubated for 5 minutes in SuperSignal™ West Pico

PLUS Chemiluminescent Substrate solution (cat# PI34580, Thermo Fisher) for immunoreactive protein reaction. Subsequently, ChemiDocTM XRS+ imager with Image Lab™ software (Bio-rad) detected the reactive bands and ImageJ software (NIH) measured individual protein band density.

Bioinformatics and statistical analysis

Proteins differentially expressed between two compared groups (p-value < 0.05) and with 1.5 or 1/1.5 fold change were deemed significant. Venn diagrams were generated from protein lists using software by Ghent University Bioinformatics and Systems Biology (http://bioinformatics.psb.ugent.be/webtools/Venn/). Heat maps were prepared using Morpheus (https://software.broadinstitute.org/morpheus). Bioinformatics analysis of proteomics datasets were performed using STRING version 11 (30), including enrichments of KEGG and Reactome pathways and UniProt keywords. Significantly enriched pathways and keywords were identified by a FDR q-value < 0.05. Pairwise comparisons for C26-WS vs. C26-MOD, C26-WS vs. C26-SEV, and C26-MOD vs. C26-SEV were prioritized for bioinformatics. For each pairwise comparison, differentially expressed proteins that increased (up-regulated) and decreased (down-regulated) were analyzed separately in the STRING database (20, 24). Hepatic glycogen, galactose, free fatty acids, triglycerides, enzyme activity, and protein expression from immunoblotting experiments were analyzed by one-way ANOVA. In the event of a significant F-test, posthoc analysis was conducted using Tukey's HSD. Significance was accepted at $p<0.05$.

Results

Phenotype of mice with moderate and severe colon-26 cancer cachexia

Tumor mass increased with cachexia severity (Table 1). Mean body weight loss was 10±1% and 22±2% in C26-MOD and C26-SEV, respectively (Table 1). Hindlimb muscle mass was ~20-30% lower in C26-MOD and C26-SEV compared to the WS groups (Table 1). Consistent with whole muscle atrophy, mean fiber area of the gastrocnemius was ~45-55% lower in C26-MOD and C26-SEV compared to WS groups (Table 1). Epididymal fat mass was lower in C26-MOD relative to PBS-WS and C26-WS (Table 1). Epididymal fat was fully depleted in C26-SEV and not measured (Table 1). The spleen was enlarged in all C26 groups by ~35-75% compared to PBS-WS (Table 1), indicating an inflammatory response to the C26 tumor. The liver was atrophied in C26-MOD and C26-SEV compared to the WS groups (Table 1).

The liver proteome in colon-26 tumor-induced cachexia

A total of 2,510 proteins were identified in liver protein extracts by LC-MS/MS, with ~50% common to all four groups, 3% exclusive to moderate cachexia, 8% unique to severe cachexia, and ~4% common to both moderate and severe cachexia (Fig. 1a, Table S2). When using PBS-WS mice as the control, 487 proteins were differentially expressed in C26-WS (up-/down-regulated: 283/204), 532 in C26-MOD (247/285), and 523 in C26-SEV (250/273) (Fig. 1b, Table S3). When using C26-WS (cancer non-cachexia) as the control, 771 proteins were differentially expressed in C26-MOD (up-/down-regulated: 355/416), and 769 in C26-SEV (341/428) (Fig. 1b,c, Table S4). Thus, selection of control impacts the detection of differentially expressed proteins in C26 cancer cachexia. When compared to C26-MOD, 557 proteins were differentially expressed in C26-SEV (up-/down-regulated: 260/297) (Fig. 1b,d, Table S4), and these proteins may be involved in the transition from moderate to severe cachexia.

A Venn diagram generated from the differentially expressed proteins in C26-WS vs. C26-MOD, and C26-MOD vs. C26-SEV, revealed an overlap region of 306 proteins (Fig. 1e, Table S5). These 306 proteins are differentially regulated at the induction of moderate cachexia, and in the transition to severe cachexia. Thus, these proteins may represent a hepatic proteomic signature needed to maintain the cachexic state. Functional annotation by KEGG pathways enrichment showed metabolic pathways, Alzheimer's disease, Parkinson's disease, Huntington's disease, lysosome, oxidative phosphorylation, and non-alcoholic fatty liver disease among the top 10 pathways (Fig. 1e). Dysregulation of mitochondrial function, particularly in its metabolic activities such as OXPHOS, are common to Alzheimer's, Huntington's, Parkinson's, and non-alcoholic fatty liver diseases, suggesting altered liver mitochondrial OXPHOS to also feature in cachexia regardless of severity. Further, 251 differentially expressed proteins were unique only in severe cachexia (Fig. 1e and Table S5), and these proteins (of the total 557 differentially expressed in severe vs. moderate) may be influential in supporting the transition from moderate to a severe presentation of the disease.

Altered mitochondrial function and substrate metabolism in moderate cachexia

Differentially expressed proteins were analyzed separately in STRING. KEGG pathways enrichment of proteins down-regulated in moderate cachexia included metabolic pathways, Alzheimer's disease, Huntington's disease, Parkinson's disease, oxidative phosphorylation, thermogenesis, and non-alcoholic fatty

liver disease among the top 10 pathways (Fig. 2a). These enriched pathways suggest a depression in liver mitochondrial OXPHOS to be associated with early cachexia. In addition, ~20% of genes involved in the TCA cycle were identified (relative to background gene count) in the down-regulated list, the largest among the represented pathways (Fig. 2a). Similarly, UniProt keywords enrichment analysis lists 'mitochondrion', 'mitochondrion inner membrane', 'oxidoreductase', 'respiratory chain', and 'electron transport' in the top 15 represented keywords from the down-regulated protein list (Table S6). The reactome pathways enrichment analysis also identified terms related to energy metabolism and mitochondrial function among the top 10 pathways (Table S6).

KEGG pathways enrichment of the up-regulated protein list in moderate cachexia show metabolic pathways, complement and coagulation cascades, carbon metabolism, biosynthesis of amino acids, protein processing in the endoplasmic reticulum, proteasome, amino sugar and nucleotide sugar metabolism, lysosome, and glycolysis/gluconeogenesis among the top 10 represented pathways (Fig. 2a). Galactose metabolism equated to ~20% of the observed/background gene count (Fig. 2a). Thus, metabolism of carbohydrates, proteins/amino acids, and nucleic acids are prominent in the livers of moderately cachexic mice. 'Mitochondrion', 'oxidoreductase', and 'electron transport' are represented in the top 20 keywords, indicating that some proteins associated with mitochondrial metabolism are increased (Table S6). 'Acute phase' appears as a top 10 keyword from the up-regulated protein data set (Table S5), consistent with the complement and coagulation cascades in the KEGG analysis. After 'thioester bond', 'acute phase' is the most represented enrichment by percentage in the up-regulated protein list with an observed/background gene count of ~30% (Table S6). The reactome pathways further supports a role of the acute phase response in moderate cachexia, with innate immune system and immune system in the top 5 (Table S6).

Transition to severe cachexia is also associated with altered energy metabolism

KEGG analysis of down-regulated proteins in severe cachexia showed metabolic pathways, proteasome, Parkinson's disease, Huntington's disease, Alzheimer's disease, oxidative phosphorylation, non-alcoholic fatty liver disease, lysosome, drug metabolism, and thermogenesis among the top 10 enriched pathways (Figs. 2b, 3a), pointing to a suppression of mitochondrial OXPHOS similar to moderate cachexia. This suppression is consistent with the UniProt analysis where 'respiratory chain', 'mitochondrion' and 'electron

transport' appear in the top 20 keywords (Table S7), and with the immunoblots of selected respiratory chain subunits (Fig. 3b). The proteasome accounted for the greatest percentage of genes represented in the KEGG analysis at ~30% observed relative to the background gene count (Fig. 2b). This aligns with the UniProt keywords analysis which indicated 'proteasome' to be the third ranked pathway by FDR, and second most observed/background gene count at 25% (Table S7). In the transition to severe cachexia, galactose metabolism was enriched in the down-regulated protein list, with a 16% observed/background gene count. This was the third highest percentage among all enriched pathways (Fig. 2b). Other glycan degradation was also an enriched KEGG pathway with observed/background gene count of 12% (Fig. 2b), supportive of ongoing carbohydrate metabolism in severe cachexia.

KEGG analysis of the up-regulated proteins yielded only 12 enriched pathways, with metabolic pathways, RNA transport, spliceosome, ribosome, and peroxisome represented in the top 5 (Fig. 2b). The UniProt keywords enrichment lists 'ribonucleoprotein', 'RNA binding', 'mRNA splicing', 'mRNA processing', 'ribosomal protein', 'spliceosome', and 'initiation factor' all represented in the top 20 (Table S7). Reactome pathways also showed predominant representation by translation and related events (Table S7). Together this points to increased processing of mRNA and protein synthesis. As in moderate cachexia, 'acute phase' remains an enriched keyword in severe cachexia (Table S8), implying an acute phase inflammatory response that persists across cachexia severity.

Hepatic carbohydrate metabolism in colon-26 tumor-induced cachexia

Bioinformatics revealed galactose metabolism to be significantly enriched in moderate cachexia, and in the transition to severe cachexia (Fig. 2a,b). Galk1, Galt, and Gale, three major proteins of the Leloir pathway responsible for interconversion of galactose and glucose, were increased in moderate cachexia and decreased from moderate to severe cachexia (Fig 4a). Their abundance, however, remained elevated in the severe state relative to non-cachexic controls (C26-WS) (Fig. 4a), suggesting that enzymes regulating galactose metabolism in moderate cachexia tends to persist into the severe state. Enrichment of these enzymes could allow for the catabolism of galactose and subsequent entry into the glycolytic pathway. Interestingly, galactose content in liver homogenates was not affected by cachexia (Fig. 4b) despite the increased expression of several key enzymes. Lysosomal α-glucosidase, which regulates glycogen catabolism in lysosomes, showed

especially robust increase based on fold-change (>7 vs. C26-WS) without altered activity (Figs. 4a,c). Consistent with glycogen breakdown, glycogen content in liver tissue homogenates are in fact decreased in cachexia (Fig. 4d), implying active glycogenolysis. Presumptive conversion of glycogen into glucose 1-phoshate and glucose 6-phosphate would suggest increased activity of glycogenolysis and glycolysis. Indeed, glycolysis is represented in the KEGG analysis of up-regulated proteins (Fig. 2a).

Given the impairment of mitochondrial OXPHOS and catabolism of carbohydrates, as well as previous suggestions of altered lactate metabolism in cancer cachexia, we explored the proteomics data sets for differentially expressed proteins involved in lactate metabolism and transport. We found decreased pyruvate dehydrogenase protein X component (Pdhx) and increased abundance of lactate dehydrogenase A chain (Ldha) according to LC-MS/MS (Table S4, Fig. 4e), changes which are expected to favor lactate formation. We also found that the lactate transporter monocarboxylate transporter 1 (Mct1) was expressed in livers of mice with both moderate and severe cachexia (Table S2, Fig. 4e). Mct1 was increased in C26-SEV compared to C26-MOD (fold-change 2.62, $P<0.05$) (Table S4), suggesting that Mct1 expression increases with cachexia severity. Collectively, these data indicate greater abundance of proteins that favor lactate formation as well as a key lactate transporter that could facilitate futile cycling of lactate between the livers of cachexic mice and the tumor.

Hepatic lipid metabolism in colon-26 tumor-induced cachexia

Previous reports of abnormal lipid metabolism in cancer cachexia agreed with our bioinformatics analysis, which showed enrichment of fatty acid metabolism (Fig. 3a, Table S8). We therefore further examined how fatty acid transport and oxidation were affected by cachexia. No differences were detected by LC/MS-MS in members of the fatty acid transport protein (FATP) family or fatty acid translocase/CD36 (Table S4), suggesting that fatty acid transport across the hepatic cell membrane was not affected by cachexia. No differences were detected in carnitine palmitoyltransferase I (Cpt1a) (Table S4), which is responsible for fatty acid transport across the mitochondrial outer membrane. There was a decrease, however, in carnitine/acylcarnitine carrier protein (Table S4), which regulates fatty acid transport across the inner membrane into the matrix. Together this suggests a possible impairment of fatty acid transport into the mitochondrial matrix.

We next generated a heatmap showing the abundance of proteins associated with fatty acid oxidation in C26 livers (Fig. 5a). Of these proteins, 20 were differentially expressed in moderate and/or severe cachexia (Fig. 5a). These differentially expressed proteins showed significant relationships with hallmark features of cancer cachexia including body weight change and muscle fiber size (Fig. 5b). They also showed significant relationships with indices of mitochondrial coupling including the respiratory control ratio, an index of OXPHOS coupling efficiency, and LEAK respiration (surrogate of proton leak) normalized to maximal OXPHOS and electron transfer system (ETS) capacities (Fig. 5b). Among the 20 differentially expressed proteins, 6 were decreased in both moderate and severe cachexia (Fig. 5a). These 6 proteins included alcohol dehydrogenase 1 (Adh1), 3-ketoacyl-CoA thiolases A (Acaa1a) and B (Acaa1b), peroxisomal L-bifunctional enzyme (Ehhadh), long chain enoyl-CoA hydratase/long-chain 3-hydroxyacyl-CoA dehydrogenase (Hadha), and long chain acyl-CoA synthetase 1 (ACSL1). With the exception of Adh1, these proteins are essential components of peroxisomal and mitochondrial beta-oxidation (Figs. 5c,d). Collectively, this profile suggests dysregulation of the beta-oxidation machinery and an impaired ability of the cachexic liver to oxidize lipids.

An impairment of hepatic lipid oxidation would be expected to cause an accumulation of lipids in the liver, which in turn may contribute to uncoupling of OXPHOS. To confirm the presence of hepatic steatosis, we assayed free fatty acids and triglycerides in liver tissue homogenates. Both were decreased in severe cachexia (Fig. 5e,f), and these events were preceded by increased acyl-CoA synthetase enzyme activity (Fig. 5g). Together this implies that lipid oxidation remains intact in the cachexic liver and that lipid accumulation and lipotoxicity is not a significant contributor to uncoupling of OXPHOS. To explore the possibility that oxidative stress to lipids contributes to uncoupling of OXPHOS in the cachexic liver, we assayed 4-HNE formation in liver tissue homogenates by immunoblotting (Fig. 6). 4-HNE formation from 15-250 kDa in the full blot was not different between groups ($P>0.05$) (Fig. 6b). However, there was significantly greater 4-HNE formation in the ~37-45 kDa bands in severe cachexia compared to non-cachexic control (Fig. 6c), suggesting the presence of some lipid peroxidation and cellular oxidative damage. Therefore, tumor-induced oxidative stress may contribute to uncoupling of OXPHOS in the cachexic liver.

Loss of acyl-CoA synthetase-1 (ACSL1) in colon-26 tumor-induced cachexia

ACSL1 is a key fatty acyl-CoA synthetase responsible for activating imported long-chain fatty acids by esterification with coenzyme A, thereby enabling further processing (e.g. by oxidation). Our proteomics analysis indicated decreased hepatic ACSL1 in moderate and severe cachexia (Fig. 5a). To validate this finding, we probed for ACSL1 in liver tissue homogenates by follow-up immunoblotting experiments. Indeed, ACSL1 expression showed a clear stepwise decrease as cachexia worsened (Figs. 7a,b). ACSL1 had strong linear relationships with percent body weight change ($r=0.874$, $P<0.01$) and myofiber size ($r=0.856$, $P<0.01$), the hallmark features of cancer cachexia (Fig. 7c). These correlations suggest greater hepatic ACSL1 in weight-stable mice with larger muscles, and lower ACSL1 in weight-losing mice with smaller muscles. ACSL1 also related linearly with the respiratory control ratio ($r=0.618$, $P<0.01$), an index of OXPHOS coupling efficiency, and inversely with LEAK respiration normalized to maximal electron transfer system capacity ($r=-0.505$, $P<0.05$) (Fig. 7c). Together these correlations suggest that weight-stable mice with larger myofibers and higher hepatic Acsl1 also had lower proton leak consistent with tighter OXPHOS coupling and energetically efficient mitochondria that dissipate less heat.

Discussion

Mass spectrometry-based proteomics have been used to profile cachexic skeletal muscle, but we are unaware of its application in cachexic liver. Here we report proteome wide changes in livers from mice with moderate and severe cancer cachexia. Of the roughly 2,500 hepatic proteins detected by mass spectrometry, 20-30% (~600-800) were identified as being differentially expressed in moderate and severe cachexia. This high number of differentially expressed proteins highlights the potential role of liver metabolism in cancer cachexia. By comparison, in the mdx-4cv mouse model of muscular dystrophy, only ~100 of the roughly 2,000 hepatic proteins detected (~5%) were found to be differentially regulated (24). The relatively lower proportion of differentially expressed proteins in muscular dystrophy could be explained by the disease being mainly a pathology of skeletal muscle, with only indirect effects on the liver. The greater percentage of hepatic proteins identified as differentially expressed in our C26 mice implies the liver, in addition to skeletal muscle, to be a significant contributor to cancer cachexia onset and progression, and an important site for targeted therapies.

To derive biological interpretations of our proteomics datasets centered on cachexia severity, we used standard bioinformatics software to analyze differentially expressed protein lists sorted by increased and

decreased abundance. Bioinformatics revealed mitochondrial OXPHOS, TCA cycle, and/or thermogenesis to be represented during the induction of moderate cachexia (Figs. 2, Tables S2-3), and in the transition to severe disease (Figs. 3, Tables S4-5), suggesting a role for hepatic mitochondrial function in the onset and progression of cancer cachexia. We previously reported loss of *in situ* OXPHOS capacity in livers from the same cohort of cachexic C26 mice (18), in line with OXPHOS being represented in down-regulated protein lists (Figs. 2-3). Interestingly, thermogenesis was also represented in down-regulated protein lists in moderate cachexia (Figs. 2a, Table S2), and in the transition to severe cachexia (Fig. 3a). If cachexic livers dissipate energy and produce heat from mitochondrial uncoupling, an increase rather than a decrease in thermogenic pathways might be expected. In phenotyping experiments, cachexic liver mitochondria show reduced P:O (i.e. lower ATP produced per molecule of oxygen consumed) (9), which suggests compromised coupling efficiency and energy wasting. Further, we previously observed loss of coupling control in livers from the same cohort of cachexic C26 mice in this study, reflecting inefficiency of OXPHOS due in part to increased LEAK respiration and Ant2, an inner membrane protein with uncoupling function (18). The current investigation also provided evidence of oxidative stress as reflected by greater 4-HNE formation (Fig. 6), which may lead to uncoupling as an ameliorative response. Together this data implies uncoupling of liver mitochondria in cachexic mice. It is possible that the enrichment of thermogenesis in down-regulated datasets reflects a compensatory effort to minimize uncoupling.

A noteworthy finding in the proteomics analysis was the identification of differentially expressed proteins in cachexic livers that would impact lactate metabolism and transport. Cachexic livers displayed decreased pyruvate dehydrogenase protein X component (Pdhx), increased lactate dehydrogenase A chain (Ldha), and increased lactate transporter Mct1 (Table S4, Fig. 4). Given that these cachexic C26 livers also demonstrated catabolism of glycogen and impaired OXPHOS, increased lactate formation and transport involving extrahepatic tissues might be an anticipated outcome. Such inter-organ lactate cycling has been previously proposed and discussed by many in recent frameworks defining potential mechanisms of cancer cachexia (1-3, 12, 13, 25, 32). Often described is a Cori cycle in which significant use of glucose by the tumor generates lactate, which is then exported and shuttled to the liver. Imported lactate is then used by the liver as a gluconeogenic substrate, which further supplies glucose to the tumor. This cycling of lactate is associated with energetic inefficiency because metabolism of glucose into lactate by the tumor generates less ATP (i.e. 2)

compared to the energy cost to convert lactate into glucose (i.e. 6 ATP) within the liver. Thus, while the premise of altered lactate metabolism involving the liver and tumor has been previously suggested, we are unaware of extensive experimental data to support these assertions specifically in cancer cachexia. Further clarification would strengthen the existence of energetically inefficient inter-organ transport between the liver and tumor, such as blood lactate concentration, the expression Mct1 and related family members as well as glucose, pyruvate, and lactate content in both the liver and cachexia inducing C26 tumors.

A novel finding in the present work was the loss of ACSL1 in cachexic livers, which to our knowledge has not been previously reported. As cachexia worsened, ACSL1 decreased in tandem. This outcome was observed in both LC-MS/MS and immunoblotting experiments (Figs. 5,7). ACSL1 is well-known for activating long chain fatty acids to form acyl-CoAs prior to further processing (e.g. oxidation) (22). ACSL1 has also been shown to positively influence mitochondrial function and coupling in several cell and disease models. In mice with heart failure, cardiac-specific overexpression of ACSL1 maintained mitochondrial oxidative energy metabolism (16). Further, overexpression of ACSL1 in Schwann cells reduced oxidative stress, normalized mitochondrial function, improved mitochondrial coupling efficiency, and reduced proton leak across the inner membrane (19). These findings have intriguing implications for cancer cachexia. Cachexic C26 livers showed evidence of oxidative stress as indicated by 4-HNE formation (Fig. 6). Further, cachexic C26 liver exhibits uncoupling due in part to reduced OXPHOS and increased LEAK respiration (18). Uncoupling of OXPHOS may contribute to cachexia-associated weight loss by dissipation of energy as heat and increase in whole body energy expenditure (Fig. 7d). The possibility exists that targeted overexpression of ACSL1 in the cachexic liver may be sufficient to improve mitochondrial function and coupling by increasing OXPHOS and/or reducing proton leak, thereby mitigating heat production and normalizing energy expenditure. ACSL1 may therefore be a candidate hepatic target for therapeutic intervention. Follow-up experiments in which ACSL1 is directly manipulated *in vivo* are warranted to better understand whether ACSL1 has the potential to slow cancer cachexia.

We note that food records for this investigation were incomplete, therefore we were unable to provide food intake data for this cohort of mice. This information is important to understand whether reduced energy intake may have contributed to cachexia-associated body weight loss, muscle atrophy, and changes to the hepatic proteome. In a previous investigation that used C26 cells from the same cell bank, food intake in

cachexic C26 mice was not different from controls (4). This finding raises the possibility that our C26 mice would also not exhibit significant anorexia, although this remains to be verified.

We conclude that the liver is an important site for targeted therapeutic strategies in cancer cachexia. Altered hepatic mitochondrial function is a common feature of both moderate and severe cancer cachexia. Proteome profiling suggests altered lactate metabolism and transport in cachexic livers, which raises the possibility of energetically inefficient lactate shuttling between the liver and tumor that elevates whole body energy expenditure and causes weight loss. Tumor-induced oxidative damage may contribute to uncoupling of cachexic liver mitochondria, which could also increase energy expenditure and weight loss. As cancer cachexia severity worsens, ACSL1 levels in the liver decline. In mice with the highest levels of ACSL1, body weight was greater, muscles were larger, and mitochondria better coupled. We propose that ACSL1 is a candidate target to consider for future experiments that aim to unravel mechanisms and therapies for cancer cachexia.

Acknowledgements

We extend our sincere thanks to Ms. Peggy Donnelly and Ms. Denise Merrill for administrative support.

Conflict of Interest

The authors declare no conflict of interest.

References

1. **Argiles JM, Busquets S, Stemmler B, and Lopez-Soriano FJ**. Cancer cachexia: understanding the molecular basis. *Nat Rev Cancer* 14: 754-762, 2014.
2. **Argiles JM, Fontes-Oliveira CC, Toledo M, Lopez-Soriano FJ, and Busquets S**. Cachexia: a problem of energetic inefficiency. *J Cachexia Sarcopenia Muscle* 5: 279-286, 2014.
3. **Argiles JM, Stemmler B, Lopez-Soriano FJ, and Busquets S**. Nonmuscle Tissues Contribution to Cancer Cachexia. *Mediators Inflamm* 2015: 182872, 2015.
4. **Assi M, Derbre F, Lefeuvre-Orfila L, and Rebillard A**. Antioxidant supplementation accelerates cachexia development by promoting tumor growth in C26 tumor-bearing mice. *Free Radic Biol Med* 91: 204-214, 2016.
5. **Barreto R, Mandili G, Witzmann FA, Novelli F, Zimmers TA, and Bonetto A**. Cancer and Chemotherapy Contribute to Muscle Loss by Activating Common Signaling Pathways. *Front Physiol* 7: 472, 2016.
6. **Bonetto A, Aydogdu T, Kunzevitzky N, Guttridge DC, Khuri S, Koniaris LG, and Zimmers TA**. STAT3 activation in skeletal muscle links muscle wasting and the acute phase response in cancer cachexia. *PLoS One* 6: e22538, 2011.
7. **Bonetto A, Rupert JE, Barreto R, and Zimmers TA**. The Colon-26 Carcinoma Tumor-bearing Mouse as a Model for the Study of Cancer Cachexia. *J Vis Exp* 2016.
8. **Diffee GM, Kalfas K, Al-Majid S, and McCarthy DO**. Altered expression of skeletal muscle myosin isoforms in cancer cachexia. *Am J Physiol Cell Physiol* 283: C1376-1382, 2002.
9. **Dumas JF, Goupille C, Julienne CM, Pinault M, Chevalier S, Bougnoux P, Servais S, and Couet C**. Efficiency of oxidative phosphorylation in liver mitochondria is decreased in a rat model of peritoneal carcinosis. *J Hepatol* 54: 320-327, 2011.
10. **Fearon K, Arends J, and Baracos V**. Understanding the mechanisms and treatment options in cancer cachexia. *Nat Rev Clin Oncol* 10: 90-99, 2013.
11. **Fearon K, Strasser F, Anker SD, Bosaeus I, Bruera E, Fainsinger RL, Jatoi A, Loprinzi C, Macdonald N, Mantovani G, Davis M, Muscaritoli M, Ottery F, Radbruch L, Ravasco P, Walsh D, Wilcock A, Kaasa S, and Baracos VE**. Definition and classification of cancer cachexia: an international consensus. *The lancet oncology* 2011.
12. **Fearon KC, Glass DJ, and Guttridge DC**. Cancer cachexia: mediators, signaling, and metabolic pathways. *Cell Metab* 16: 153-166, 2012.
13. **Friesen DE, Baracos VE, and Tuszynski JA**. Modeling the energetic cost of cancer as a result of altered energy metabolism: implications for cachexia. *Theor Biol Med Model* 12: 17, 2015.
14. **Fukawa T, Yan-Jiang BC, Min-Wen JC, Jun-Hao ET, Huang D, Qian CN, Ong P, Li Z, Chen S, Mak SY, Lim WJ, Kanayama HO, Mohan RE, Wang RR, Lai JH, Chua C, Ong HS, Tan KK, Ho YS, Tan IB, Teh BT, and Shyh-Chang N**. Excessive fatty acid oxidation induces muscle atrophy in cancer cachexia. *Nat Med* 22: 666-671, 2016.
15. **Gallagher IJ, Jacobi C, Tardif N, Rooyackers O, and Fearon K**. Omics/systems biology and cancer cachexia. *Semin Cell Dev Biol* 54: 92-103, 2016.
16. **Goldenberg JR, Carley AN, Ji R, Zhang X, Fasano M, Schulze PC, and Lewandowski ED**. Preservation of Acyl Coenzyme A Attenuates Pathological and Metabolic Cardiac Remodeling Through Selective Lipid Trafficking. *Circulation* 139: 2765-2777, 2019.
17. **Goncalves MD, Hwang SK, Pauli C, Murphy CJ, Cheng Z, Hopkins BD, Wu D, Loughran RM, Emerling BM, Zhang G, Fearon DT, and Cantley LC**. Fenofibrate prevents skeletal muscle loss in mice with lung cancer. *Proc Natl Acad Sci U S A* 115: E743-E752, 2018.
18. **Halle JL, Pena GS, Paez HG, Castro AJ, Rossiter HB, Visavadiya NP, Whitehurst MA, and Khamoui AV**. Tissue-specific dysregulation of mitochondrial respiratory capacity and coupling control in colon-26 tumor-induced cachexia. *Am J Physiol Regul Integr Comp Physiol* 2019.
19. **Hinder LM, Figueroa-Romero C, Pacut C, Hong Y, Vivekanandan-Giri A, Pennathur S, and Feldman EL**. Long-chain acyl coenzyme A synthetase 1 overexpression in primary cultured Schwann cells prevents long chain fatty acid-induced oxidative stress and mitochondrial dysfunction. *Antioxid Redox Signal* 21: 588-600, 2014.
20. **Hong G, Zhang W, Li H, Shen X, and Guo Z**. Separate enrichment analysis of pathways for up- and downregulated genes. *J R Soc Interface* 11: 20130950, 2014.
21. **Khamoui AV, Park BS, Kim DH, Yeh MC, Oh SL, Elam ML, Jo E, Arjmandi BH, Salazar G, Grant SC, Contreras RJ, Lee WJ, and Kim JS**. Aerobic and resistance training dependent skeletal muscle plasticity in the colon-26 murine model of cancer cachexia. *Metabolism* 65: 685-698, 2016.

22. **Li LO, Ellis JM, Paich HA, Wang S, Gong N, Altshuller G, Thresher RJ, Koves TR, Watkins SM, Muoio DM, Cline GW, Shulman GI, and Coleman RA**. Liver-specific loss of long chain acyl-CoA synthetase-1 decreases triacylglycerol synthesis and beta-oxidation and alters phospholipid fatty acid composition. *J Biol Chem* 284: 27816-27826, 2009.
23. **Murphy KT, Chee A, Trieu J, Naim T, and Lynch GS**. Importance of functional and metabolic impairments in the characterization of the C-26 murine model of cancer cachexia. *Disease models & mechanisms* 5: 533-545, 2012.
24. **Murphy S, Zweyer M, Henry M, Meleady P, Mundegar RR, Swandulla D, and Ohlendieck K**. Proteomic profiling of liver tissue from the mdx-4cv mouse model of Duchenne muscular dystrophy. *Clin Proteomics* 15: 34, 2018.
25. **Porporato PE**. Understanding cachexia as a cancer metabolism syndrome. *Oncogenesis* 5: e200, 2016.
26. **Reid J, McKenna HP, Fitzsimons D, and McCance TV**. An exploration of the experience of cancer cachexia: what patients and their families want from healthcare professionals. *European journal of cancer care* 19: 682-689, 2010.
27. **Shum AM, Fung DC, Corley SM, McGill MC, Bentley NL, Tan TC, Wilkins MR, and Polly P**. Cardiac and skeletal muscles show molecularly distinct responses to cancer cachexia. *Physiol Genomics* 47: 588-599, 2015.
28. **Shum AMY, Poljak A, Bentley NL, Turner N, Tan TC, and Polly P**. Proteomic profiling of skeletal and cardiac muscle in cancer cachexia: alterations in sarcomeric and mitochondrial protein expression. *Oncotarget* 9: 22001-22022, 2018.
29. **Stephens NA, Gallagher IJ, Rooyackers O, Skipworth RJ, Tan BH, Marstrand T, Ross JA, Guttridge DC, Lundell L, Fearon KC, and Timmons JA**. Using transcriptomics to identify and validate novel biomarkers of human skeletal muscle cancer cachexia. *Genome medicine* 2: 1, 2010.
30. **Szklarczyk D, Gable AL, Lyon D, Junge A, Wyder S, Huerta-Cepas J, Simonovic M, Doncheva NT, Morris JH, Bork P, Jensen LJ, and Mering CV**. STRING v11: protein-protein association networks with increased coverage, supporting functional discovery in genome-wide experimental datasets. *Nucleic Acids Res* 47: D607-D613, 2019.
31. **Twelkmeyer B, Tardif N, and Rooyackers O**. Omics and cachexia. *Curr Opin Clin Nutr Metab Care* 20: 181-185, 2017.
32. **Vaughan VC, Martin P, and Lewandowski PA**. Cancer cachexia: impact, mechanisms and emerging treatments. *J Cachexia Sarcopenia Muscle* 4: 95-109, 2013.
33. **von Haehling S, and Anker SD**. Cachexia as a major underestimated and unmet medical need: facts and numbers. *J Cachexia Sarcopenia Muscle* 1: 1-5, 2010.
34. **White JP, Baynes JW, Welle SL, Kostek MC, Matesic LE, Sato S, and Carson JA**. The regulation of skeletal muscle protein turnover during the progression of cancer cachexia in the Apc(Min/+) mouse. *PLoS One* 6: e24650, 2011.

Supplementary Table S1

https://figshare.com/s/d591441d6e108e95c900

https://doi.org/10.6084/m9.figshare.11803266

Supplementary Table S2

https://figshare.com/s/12e1a8c8a969a2f62bb9

https://doi.org/10.6084/m9.figshare.11340920

Supplementary Table S3

https://figshare.com/s/60495c0f448a4b7d0210

https://doi.org/10.6084/m9.figshare.11340944

Supplementary Table S4

https://figshare.com/s/e025d24b3419cddf2f78

https://doi.org/10.6084/m9.figshare.11340950

Supplementary Table S5

https://figshare.com/s/78f8a8fcc9ab4da11bed

https://doi.org/10.6084/m9.figshare.11340953

Supplementary Table S6

https://figshare.com/s/9026f034fee9f1f5fa5f

https://doi.org/10.6084/m9.figshare.11340956

Supplementary Table S7

https://figshare.com/s/dfbba7ddce2f5aa240d4

https://doi.org/10.6084/m9.figshare.11340959

Supplementary Table S8

https://figshare.com/s/912870d3873c7bbbfba2

https://doi.org/10.6084/m9.figshare.11340962

Figure Legends

Figure 1. Moderate and severe cancer cachexia share ~300 differentially expressed proteins in liver

(a) Venn diagram illustrating the total number of proteins identified in each group, and the number of shared proteins between groups. A total of 2,510 proteins were identified by liquid chromatography-tandem mass spectrometry. Livers were assayed from PBS Weight-Stable (PBS-WS, n=4), C26 Weight-Stable (C26-WS, n=6), C26 Moderate (C26-MOD, n=7), and C26 Severe (C26-SEV, n=6). (b) Number of differentially expressed proteins that are up- or down-regulated for each paired comparison. (c-d) Heat maps generated from differentially expressed proteins during the induction of moderate cachexia (C26-WS vs. C26-MOD), and the transition from moderate to severe presentation of the disease (C26-MOD vs. C26-SEV). (e) Venn diagram generated by using differentially expressed proteins detected during the induction of moderate cachexia (C26-WS vs. C26-MOD), and the transition from moderate to severe presentation of the disease (C26-MOD vs. C26-SEV). The 306 shared proteins in the overlap region may be necessary to maintain the cachexic state, and are hypothesized to represent a proteomic signature of cachexia. KEGG pathways enrichment of these differentially expressed proteins was conducted with STRING. The top 15 KEGG pathways are shown.

Figure 2. KEGG pathways enrichment of differentially expressed proteins in moderate cachexia

(a) KEGG pathways enrichment of down-regulated and up-regulated protein datasets in moderate cachexia. Enriched KEGG pathways were identified from differentially expressed hepatic proteins in C26 Moderate cachexia (C26-MOD, n=7) relative to C26 Weight-Stable (C26-WS, n=6) using the STRING database. (b) KEGG pathways enrichment of down-regulated and up-regulated protein datasets in the transition from moderate to severe cachexia. Enriched KEGG pathways were identified from differentially expressed hepatic proteins in C26 Severe (C26-SEV, n=6) relative to C26 Moderate (C26-MOD, n=7) using the STRING database. Values adjacent to individual bars are the percentage of identified genes from the imported protein list relative to the background gene count for that pathway, and the false discovery rate q-value.

Figure 3. KEGG pathways enrichment of differentially expressed proteins in severe cachexia

(a) KEGG pathways enrichment of down-regulated and up-regulated protein datasets in severe cachexia. Enriched pathways were identified from differentially expressed hepatic proteins in C26 mice with severe cachexia (C26-SEV, n=6) relative to C26 Weight-Stable (C26-WS, n=6) using the STRING database. Values adjacent to individual bars are the percentage of identified genes from the imported protein list relative to the background gene count for that pathway, and the false discovery rate q-value. (b) Top panel is showing immunoblots for complex I-V subunits of the mitochondrial respiratory chain probed in liver tissue homogenates. Bottom figure is showing expression of the complex I-V subunits normalized to GAPDH. Data presented as mean ± SE. Tissues assayed from PBS Weight-Stable (n=4), C26 Weight-Stable (n=6), C26 Moderate (n=7), and C26 Severe (n=6). Differences determined by one-way ANOVA. $p<0.05$ (*), $p<0.01$ (**), $p<0.001$ (***).

Figure 4. Hepatic carbohydrate metabolism in colon-26 tumor-induced cachexia.

(a) Fold-changes for differentially expressed proteins involved in galactose metabolism. Arrows represent increased or decreased abundance and values indicate the magnitude of the fold-change. Shown are proteins that were differentially expressed in moderate cachexia (C26-WS vs. C26-MOD), severe cachexia (C26-WS vs. C26-SEV), or the transition from moderate to severe cachexia (C26-MOD vs. C26-SEV). (b-d) Galactose, α-glucosidase enzyme activity, and glycogen content in liver homogenates were measured by fluorometry and spectrophotometry. Tissues assayed from C26 Weight-Stable (n=6), C26 Moderate (n=7), and C26 Severe (n=6). Differences determined by one-way ANOVA. $p<0.05$ (*). (e) Summary of findings involving carbohydrate metabolism in the cachexic liver. LC-MS/MS indicated decreased pyruvate dehydrogenase protein X component (Pdhx), increased lactate dehydrogenase A chain (Ldha), and increased lactate transporter Mct1. Cachexic C26 livers also demonstrated catabolism of glycogen and impaired OXPHOS, therefore increased lactate formation and transport involving extrahepatic tissues (e.g. the tumor) are expected. Such inter-organ lactate cycling is associated with energetic inefficiency because metabolism of glucose into lactate by the tumor generates less ATP (i.e. 2) compared to the energy cost to convert lactate into glucose (i.e. 6 ATP) within the liver.

Figure 5. Hepatic lipid metabolism in colon-26 tumor-induced cachexia.

(a) Heatmap of hepatic proteins involved in lipid oxidation from C26 weight-stable mice (C26-WS, n=6), C26 mice with moderate cachexia (C26-MOD, n=7), and C26 mice with severe cachexia (C26-SEV, n=6). (b) Of the hepatic proteins shown in the heatmap, 20 were differentially expressed in moderate cachexia (C26-WS vs. C26-MOD), severe cachexia (C26-WS vs. C26-SEV), or the transition from moderate to severe cachexia (C26-MOD vs. C26-SEV). These 20 differentially expressed proteins were correlated with hallmark features of cancer cachexia and indicators of mitochondrial coupling, as shown in the table color-coded by maximum (red) and minimum (blue) Pearson-r correlation coefficients. The hallmark features of cachexia were percent body weight change, and muscle fiber cross-sectional area (CSA) determined by hematoxylin staining and standard morphometric techniques. Indicators of mitochondrial coupling were derived from high-resolution respirometry experiments including the respiratory control ratio (RCR), and LEAK respiration normalized to maximal oxidative phosphorylation (OXPHOS) and electron transfer system (ETS) capacities. Weight change, myofiber size, and respiration data were previously published (18). $p<0.05$ (*), $p<0.01$ (**), $p=0.05$-0.09 (^) (c-d) Proteins regulating mitochondrial and peroxisomal beta-oxidation of fatty acids are differentially expressed in moderate (C26-WS vs. C26-MOD) and severe cachexia (C26-WS vs. C26-SEV). (e-g) Total free fatty acids, triglycerides, and acyl-CoA synthetase enzyme activity in liver homogenates from C26-WS, C26-MOD, and C26-SEV measured by fluorometry. Differences determined by one-way ANOVA. $p<0.05$ (*), $p<0.01$ (**).

Figure 6. Hepatic lipid peroxidation and oxidative stress in colon-26 tumor-induced cachexia.

(a) Immunoblots showing 4-HNE formation in the full blot from 15-250 kDa probed in liver tissue homogenates. (b) 4-HNE formation in the full blot determined by expression of bands from 15-250 kDa normalized to GAPDH. (c) 4-HNE formation of bands from ~37-45 kDa normalized to GAPDH. Data presented as mean ± SE. Tissues assayed from PBS Weight-Stable (n=4), C26 Weight-Stable (n=6), C26 Moderate (n=7), and C26 Severe (n=6). Differences determined by one-way ANOVA. $p<0.05$ (*).

Figure 7. Loss of hepatic ACSL1 in colon-26 tumor-induced cachexia.

(a) Immunoblots showing Acyl-CoA synthetase-1 (ACSL1) expression in liver tissue homogenates. (b) ACSL1 expression normalized to GAPDH. Data presented as mean ± SE. Tissues assayed from PBS Weight-Stable

(n=4), C26 Weight-Stable (n=6), C26 Moderate (n=7), and C26 Severe (n=6). Differences determined by one-way ANOVA. $p<0.05$ (*), $p<0.01$ (**), $p<0.001$ (***). (c) Associations of ACSL1 with percent body weight change, myofiber size, respiratory control ratio (RCR), and LEAK respiration in the complex I supported state normalized to maximal electron transfer system capacity (ETS). Weight change, myofiber size, and respiration data were previously published (18) and used here for correlative purposes. (d) Proposed mechanisms linking hepatic metabolism to cancer cachexia. In response to tumor-secreted factors, the cachexic liver is subject to oxidative stress as indicated by greater 4-HNE formation, which could contribute to uncoupling of mitochondrial oxidative phosphorylation (OXPHOS) and lead to an increase in energy expenditure and weight loss. The cachexic liver also shows decreased levels of ACSL1. ACSL1 has been shown to protect against oxidative stress and positively influence mitochondrial function and coupling in several cell and disease models. Loss of hepatic ACSL1 may therefore alter metabolism of the liver and contribute to cachexia-associated abnormalities.

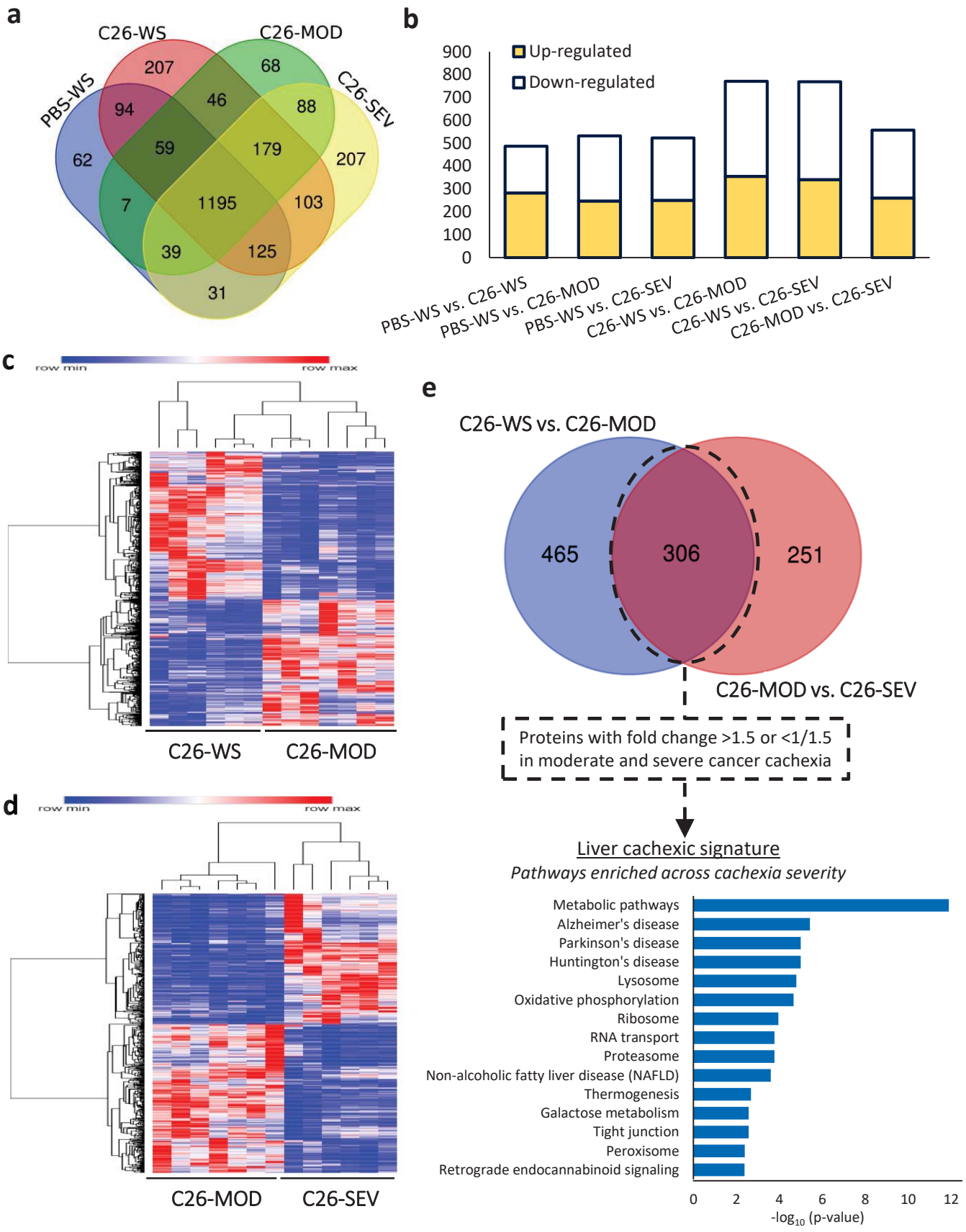

Figure 1

a

C26-WS vs. C26-MOD

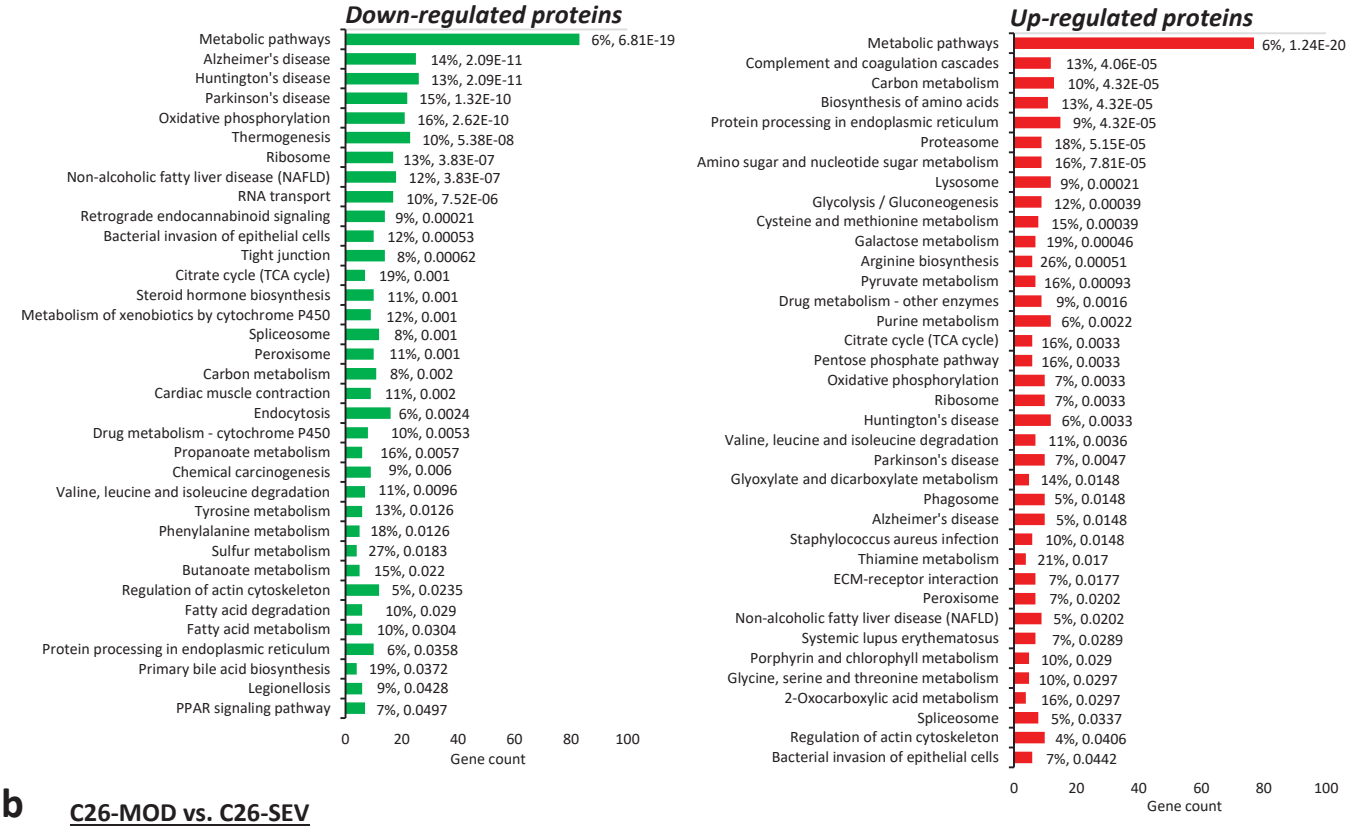

b

C26-MOD vs. C26-SEV

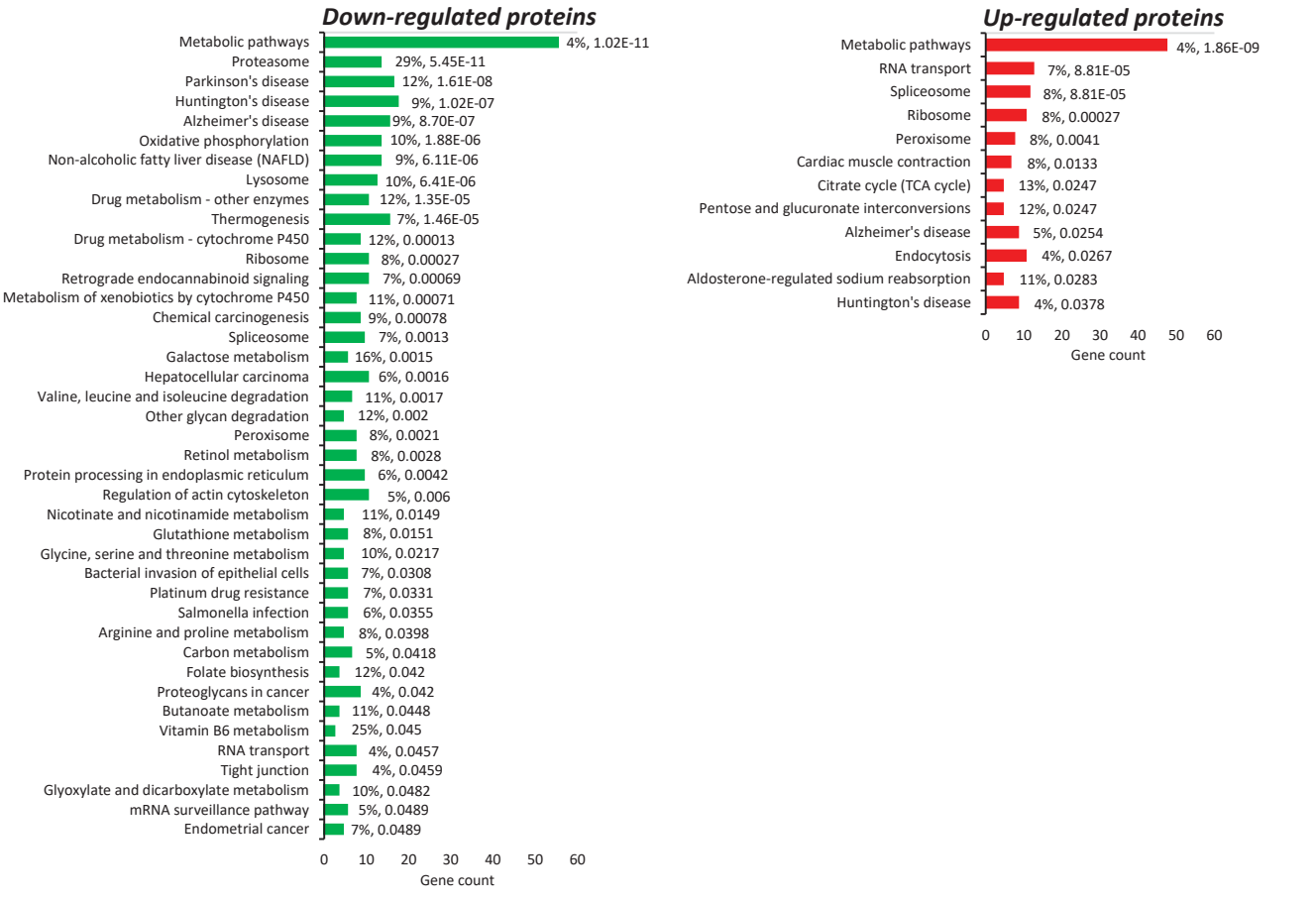

Figure 2

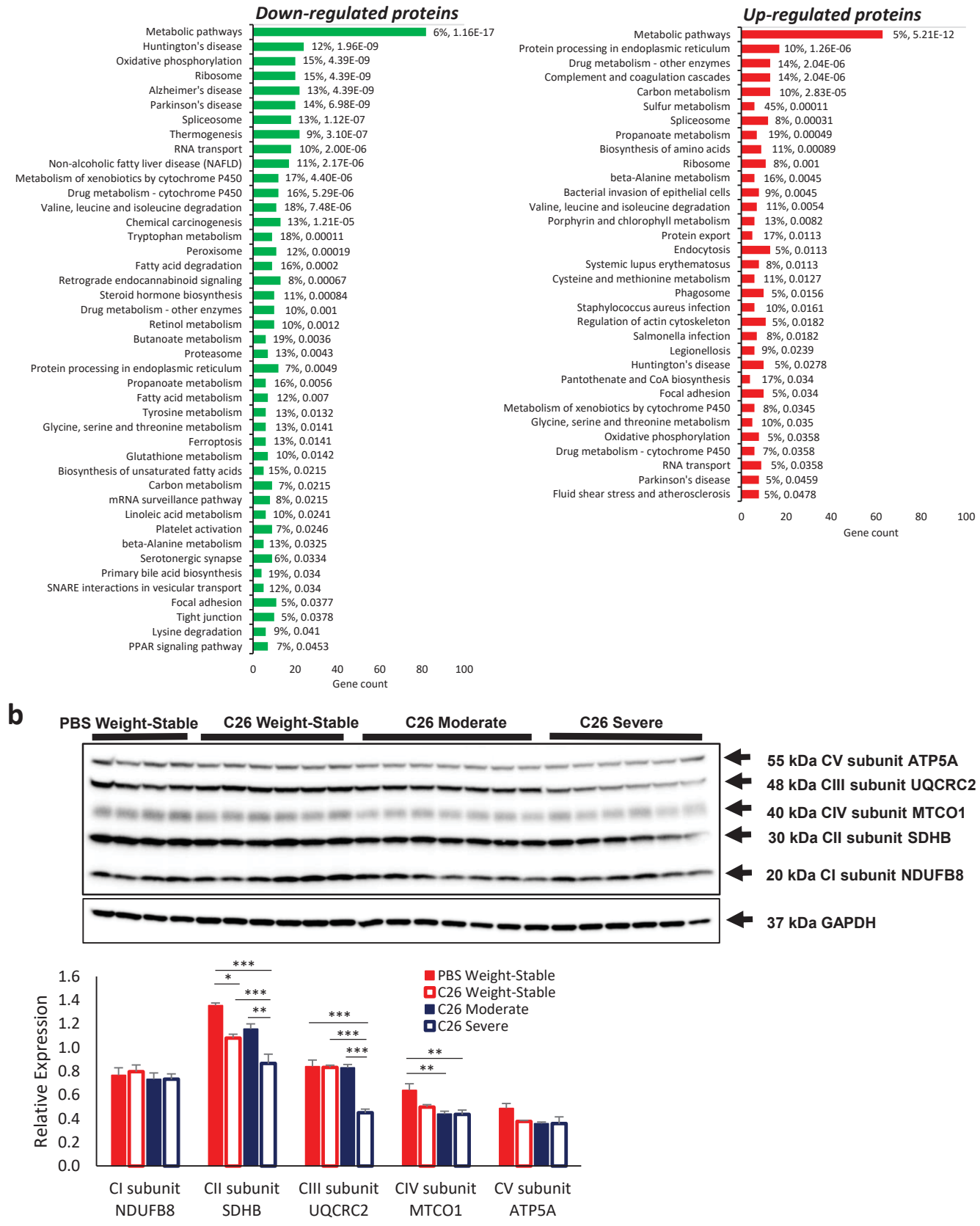

Figure 3

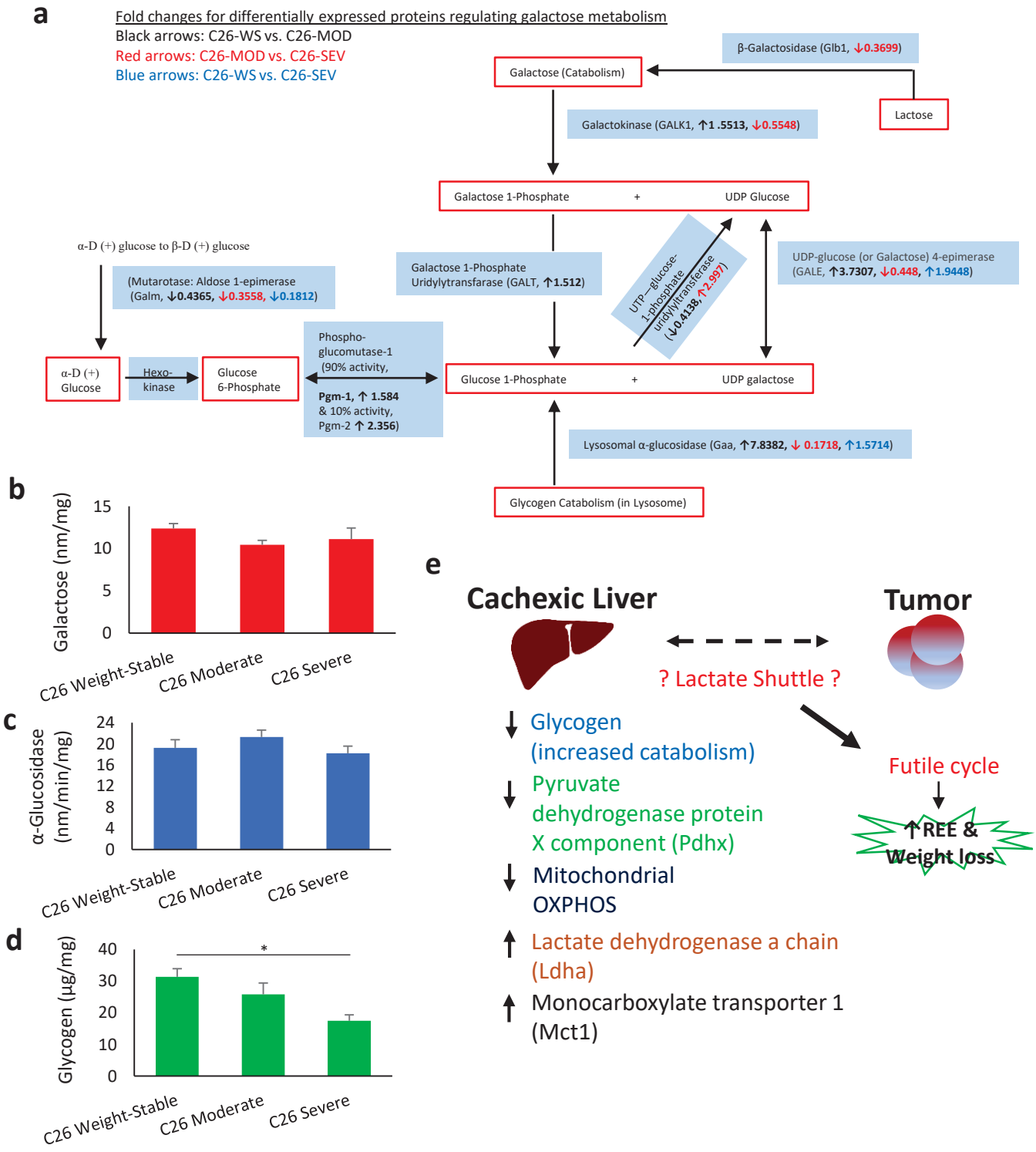

Figure 4

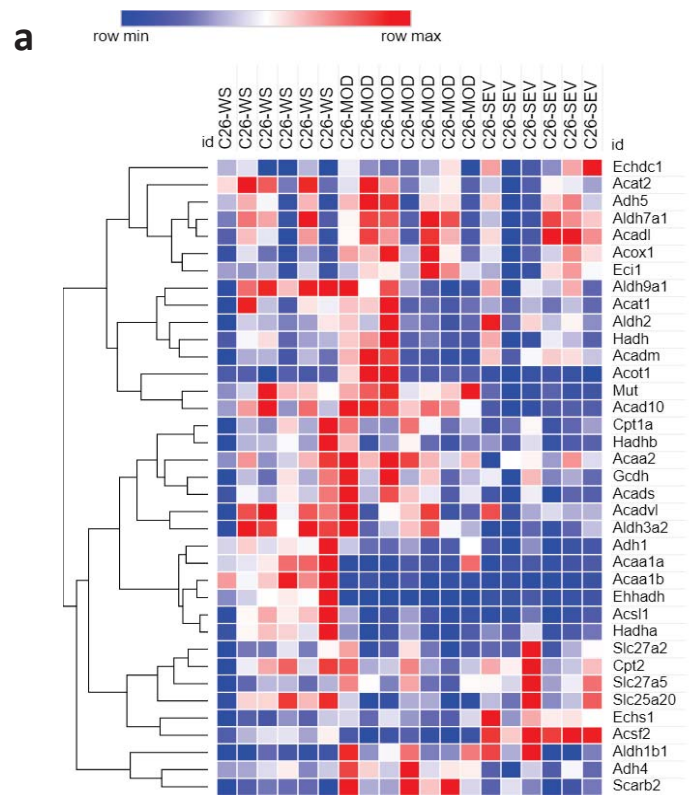

b

	% Weight Change	Fiber CSA	RCR	LEAK/ OXPHOS	LEAK/ ETS
Acsl1	0.59 **	0.49 *	0.28	-0.42 *	-0.44 *
Adh1	0.60 **	0.17	0.20	-0.17	-0.26
Acaa1a	0.76 **	0.63 **	0.39 ^	-0.28	-0.29
Acaa1b	0.69 **	0.36	-0.10	0.12	-0.05
Adh4	-0.06	-0.46 *	-0.17	0.28	0.04
Acads	0.17	-0.32	-0.03	0.04	-0.16
Aldh1b1	-0.52 *	-0.70 **	-0.51 *	0.46 *	0.39 ^
Echs1	-0.58 **	-0.38 ^	-0.41 ^	0.13	0.43 *
Ehhadh	0.68 **	0.55 *	0.14	-0.32	-0.30
Aldh3a2	0.45 *	0.46 *	0.50 *	-0.50 *	-0.50 *
Acadm	-0.29	-0.23	-0.26	0.15	0.19
Slc25a20	-0.01	-0.23	-0.56 *	0.23	0.20
Hadha	0.36 *	0.06	-0.25	-0.03	-0.07
Scarb2	-0.29	-0.51 *	-0.02	0.15	-0.05
Slc27a5	-0.43 *	-0.42 ^	-0.23	0.04	0.07
Eci1	-0.20	-0.26	0.19	0.09	0.09
Acsf2	-0.45 *	-0.22	-0.62 **	0.17	0.41 *
Mut	0.06	-0.33	-0.28	0.53 **	0.29
Acot1	0.22	0.24	0.53 **	-0.40 ^	-0.44 *
Acad10	0.45 *	0.31	0.46 *	-0.15	-0.35

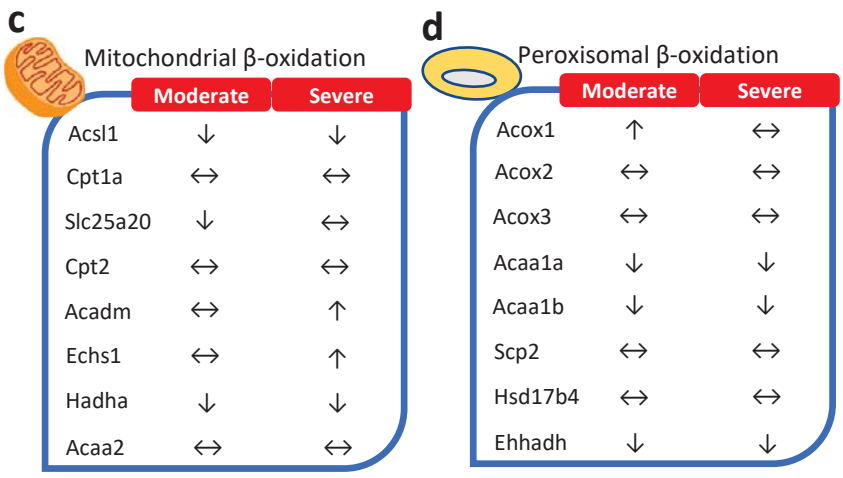

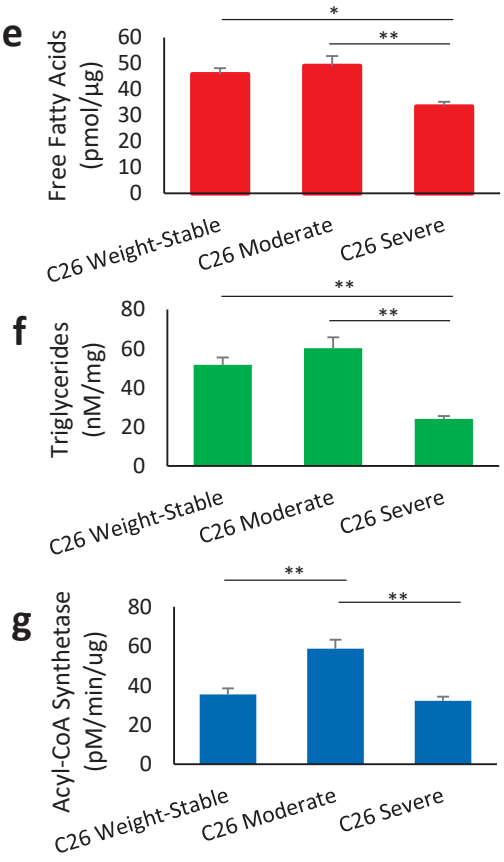

Figure 5

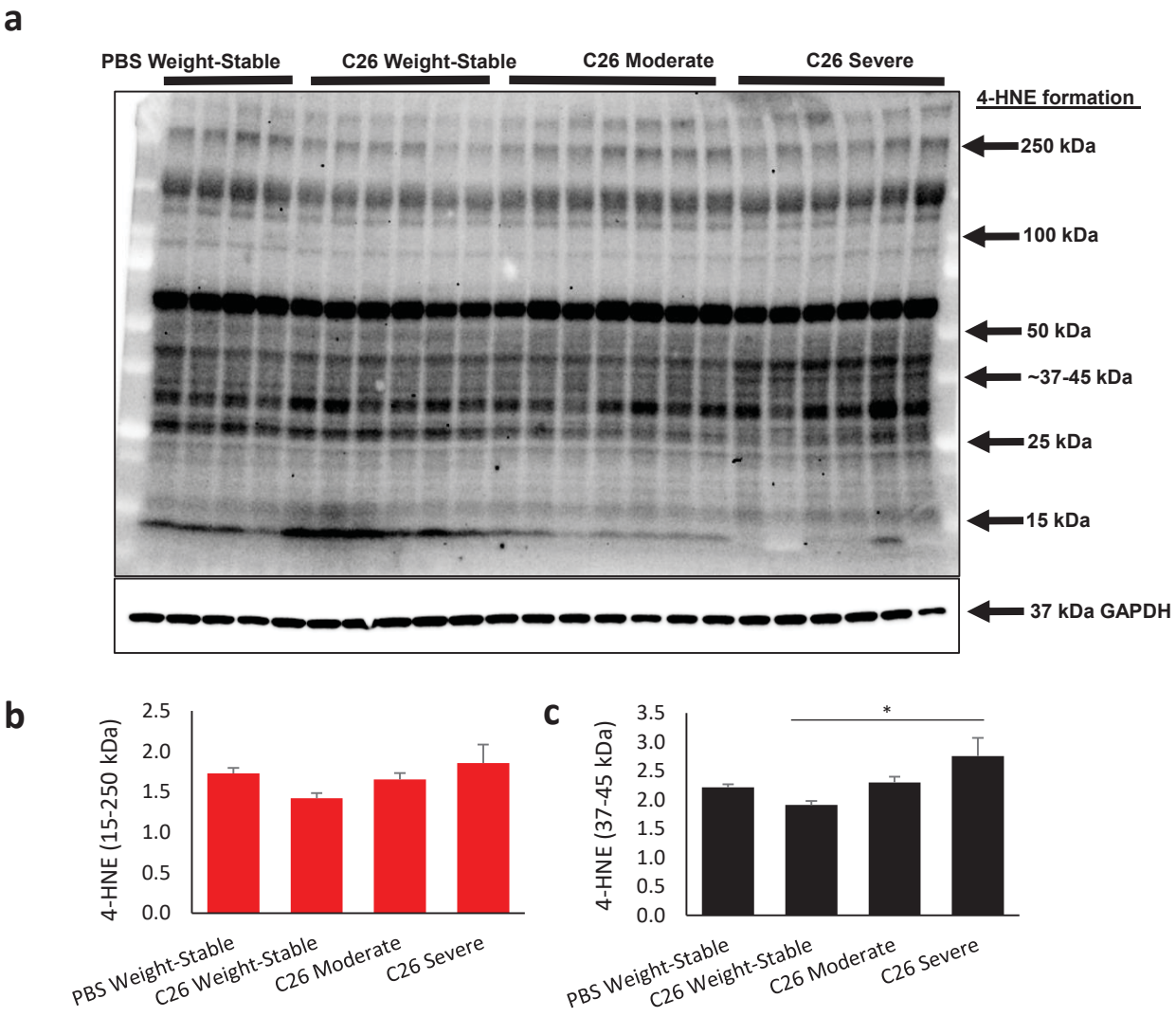

Figure 6

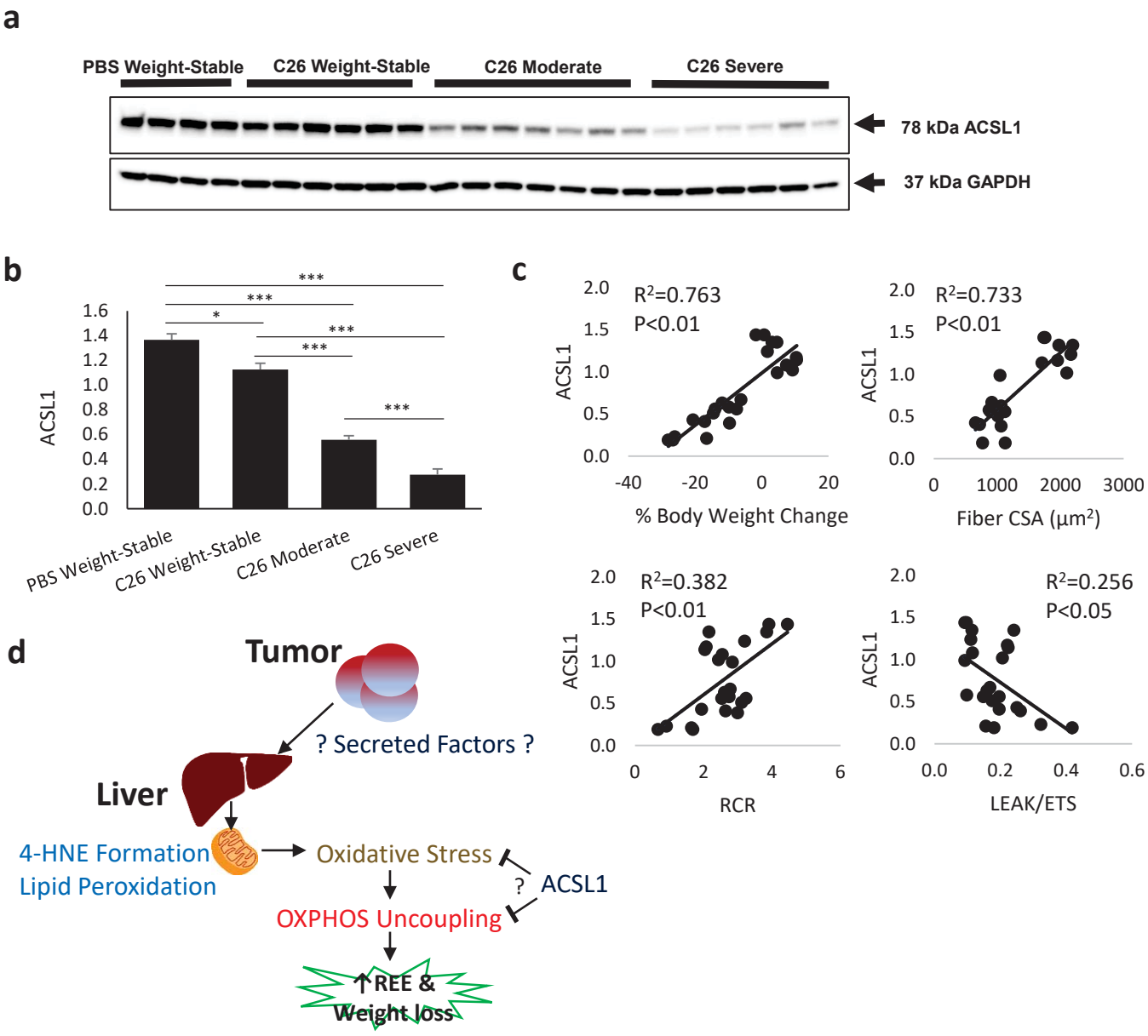

Figure 7

Table 1. Phenotype of mice with moderate and severe colon-26 tumor-induced cachexia

	PBS Weight-Stable	C26 Weight-Stable	C26 Moderate Cachexia	C26 Severe Cachexia
Tumor weight (g)	--	0.4±0.1 $^{\#\#, @@@}$	1.1±0.1 $^{@@@}$	2.1±0.2
Body weight change (%)	1±1 $^{\#\#\#, @@@}$	8±1 $^{\#\#\#, @@@}$	-10±1 $^{@@@}$	-22±2
Quadriceps (mg)	166±10 $^{\#, @@}$	164±7 $^{\#, @@}$	132±9	121±4
Plantaris (mg)	13.1±0.7 $^{\#\#, @}$	12.4±0.3 $^{\#, @}$	10.0±0.7	10.3±0.4
Gastrocnemius (mg)	112±2 $^{\#\#, @@@}$	110±3 $^{\#\#, @@@}$	90±3	84±4
Fiber CSA (μm^2)	1,965±126 $^{\#\#\#, @@@}$	1,758±189 $^{\#\#\#, @@@}$	994±37	820±105
Epididymal fat (mg)	173±26 $^{\#\#\#}$	183±12 $^{\#\#\#}$	58±9	ND
Spleen (mg)	89±4 $^{\wedge, \#\#}$	128±7	155±8	119±12
Liver (mg)	1,598±65 $^{\#\#, @@}$	1,607±41 $^{\#\#, @@}$	1,311±44	1,311±44

The phenotype for this cohort of mice has been reported previously (18) and are provided here for descriptive purposes. CSA, cross-sectional area of the gastrocnemius. ND, not detected. n=4-7/group. Data are mean ± SE. Differences determined by one-way ANOVA. P<0.05 ($^{\wedge}$) vs. C26 Weight-Stable. P<0.05 ($^{\#}$), P<0.01 ($^{\#\#}$), P<0.001 ($^{\#\#\#}$) vs. C26 Moderate Cachexia. P<0.05 ($^{@}$), P<0.01 ($^{@@}$), P<0.001 ($^{@@@}$) vs. C26 Severe Cachexia.